SnO$_2$-SiO$_2$ 1D Core-Shell Nanowires Heterostructures for Selective Hydrogen Sensing

Muhammad Hamid Raza[1], Navpreet Kaur[2], Elisabetta Comini[2*], Nicola Pinna[1*]

1 -Institut für Chemie and IRIS Adlershof, Humboldt-Universität zu Berlin, Brook-Taylor-Str. 2, 12489 Berlin, Germany

2 -Sensor Lab, Department of Information Engineering, University of Brescia, Via Valotti 9, 25133 Brescia, Italy

* Corresponding Author E-mail: elisabetta.comini@unibs.it, nicola.pinna@hu-berlin.de

Abstract

SnO$_2$ is one of the most employed n-type semiconducting metal oxide (SMOX) in chemo-resistive gas-sensing although it presents serious limitations due to a low selectivity. Herein, we introduce one-dimensional (1D) SnO$_2$-SiO$_2$ core-shell nanowires (CSNWs). SnO$_2$ nanowires (NWs) are synthesized by vapor–liquid–solid deposition and the amorphous SiO$_2$-shell layer with varying thicknesses (1.8–10.5 nm) was grown by atomic layer deposition (ALD). SiO$_2$-coated SnO$_2$ CSNWs show lower baseline conductance as compared to the Pristine SnO$_2$ NWs, due to an enhancement of the electron depletion layer. The SnO$_2$-SiO$_2$/N CSNWs (N representing the number of SiO$_2$ ALD cycles) sensors show a dramatic improvement of the selectivity towards hydrogen. Moreover, the sensing-response markedly depends on the thickness of the SiO$_2$-shell layer and the working temperature. The SnO$_2$-SiO$_2$/60 CSNWs sensor ($ca.$ 4.8 nm SiO$_2$ shell thickness) was the best performing sensor in terms of selectivity and sensitivity exhibiting a response of 160 ($ca.$ 7-folds higher than the pristine SnO$_2$ NWs) towards 500 ppm of hydrogen at 500 °C with a lower detection limit at ppb-level (0.082 ppm). The selectivity and enhanced sensing-response are related to the masking effect of the SiO$_2$ shell and an increased in the width of the electron depletion layer due to the strong electronic coupling between the SnO$_2$ core and SiO$_2$-shell layer, respectively. The remarkable sensing performances of the SnO$_2$-SiO$_2$/N CSNWs can be attributed to the homogeneous and conformal SiO$_2$ shell layer by ALD, electronic coupling between the core and the shell, the optimized shell thickness and high surface area provided by the 1D SnO$_2$ NWs network.

KEYWORDS

SnO$_2$-SiO$_2$, atomic layer deposition, shell thickness, H$_2$ selectivity, core-shell nanowires

Introduction

Hydrogen is extensively used in numerous fields such as aerospace, chemical industry, fuel cells, electronics and civil engineering.[1] Taking into account the very low and wide flammable and explosive range of H_2 concentrations (4–75%), and its colorless and odorless properties, the management and safety of hydrogen raise a demanding challenge.[2] Therefore, it is essential to monitor the leakage of hydrogen at trace levels.[3-5]

SnO_2 is one of the most reported *n*-type semiconducting metal oxide (SMOX) employed in chemo-resistive gas-sensing, due to its wide band gap (3.6 eV at 300 K), low material cost, fast response, stability and simplicity.[6-7] However, SnO_2-based gas sensors are limited by their low selectivity, e.g. interference with other reducing gases such as ethanol, methane and carbon monoxide that prevents accurate hydrogen detection.[8] It has been observed that SnO_2-based gas sensors show effective improvements in their gas-sensing properties by employing various SnO_2 nanostructures in combination with secondary-materials such as by doping,[9] surface modification with noble metals catalysts (e.g. Pt, Pd, Au, Ag)[7,10-12] and metal oxides (ZnO, In_2O_3, NiO).[8,13-14] Moreover, SMOX loaded with other materials can exhibit enhanced sensing characteristics due to modified transducer/receptor functions. Finally, nanoscale heterojunctions can further increase the gas-sensing responses due to the Fermi-level effect.[15-17]

One of the efficient methods to enhance selectivity of chemo-resistive gas sensors is to use a catalytic membrane on top of the core-materials.[18-19] For example, it is possible by using platinum, palladium and nickel membranes to enhance the hydrogen and ethanol selectivity of a sensor in presence of other interfering gases.[20-21] Additionally, some metal organic frameworks (MOFs) materials such as zeolitic imidazolate frameworks (ZIF-67 and ZIF-8) have been reported to act as molecular sieves to enhance the selectivity of gas-sensors.[22-24] Especially, high response-signals were recorded for low concentration of H_2, whereas no significant response toward other interfering gases such as benzene, toluene, acetone and ethanol were detected.[22] On the other hand, MOFs are not stable at the typical operating temperature of SnO_2-based gas sensors (around 400°C). Likewise, the use of a SiO_2 amorphous film onto an active substrate (mostly SnO_2) has also been reported to improve the selectivity for hydrogen sensing.[19,25] In these sensors, the amorphous SiO_2 film apparently acts as a "molecular sieve", effectively decreasing the diffusion of gases having larger molecular sizes than H_2, leading to an improved selectivity to H_2.[26]

SiO_2 coatings onto the SMOX are typically synthesized by chemical vapour deposition (CVD) or soft-chemistry approaches such as the sol-gel process using different silanes such as ethoxysilanes, hexamethyldisiloxane (HMDS), triethoxymethylsilane (TEMS) and ethoxy-trimethylsilane (ETMS), dirthoxydimethylsilane (DEMS) by dip- or spin-coating.[19,26-30] Even though an improvement in the selectivity towards H_2 detection has been reported by using SiO_2–SnO_2 based materials, most of these reported nanomaterials lack in a fine control over the properties of the SiO_2 layer in terms of homogeneity, conformality and thickness.[26] As a matter of fact, only with a precise control of the SiO_2 coating, it would be possible to address fundamental questions like (i) how the SiO_2–shell layer acts as a molecular sieve, (ii) how the thickness of the SiO_2 coating influences the sensitivity and selectivity and ultimately leads to an enhancement of the gas-sensing performance, and (iii) what is the transducing mechanism of the heterostructures. Hence, only well-defined hierarchical nanostructures can be used to propose clear structure-properties relationship.[8,16,30-31]

The choice of active sensing material where such a masking layer can be applied is another significant factor. In recent years, due to their peculiar morphology and high surface-to-volume ratio, various one-dimensional (1D) nanostructures (e.g., nanorods, nanowires and nanobelts) have been synthesized and studied as the active material in state of the art metal oxide gas-sensors.[10,32-35] These 1D nanowires provide a large number of active surface sites for the adsorption of gas molecules due to their high surface area.[36-40] For examples, one of our recent study has shown that SnO_2 based C-S heterostructures such as SnO_2-NiO showed improved properties towards hydrogen gas-sensing as compared to pristine SnO_2 nanostructures.[8] In that case, the enhanced sensing-response after the NiO-coatings was assigned to the formation of a *p-n* junction and to the modulation of space charge region. Moreover, it was demonstrated that the sensing-response was dependent on the thickness of the NiO-shell layer.[8] Therefore, also in this study 1D SnO_2 nanowires (NWs) are chosen as the model material to study the role of SiO_2-coating thickness.

In this study, we describe the fabrication of well-defined hierarchical 1D SnO_2 (core)/SiO_2 (shell) core-shell nanowires (CSNWs) with different thicknesses of the shell layer directly onto the sensing device using a vapor–liquid–solid (VLS) and atomic layer deposition techniques. Since it is crucial to control the size of the nanowires and the thickness (on the order of a few nanometers) of the shell layer deposited onto the core substrate, atomic layer deposition (ALD) was chosen as a deposition technique in this study. ALD shows an atomic scale level control over the thickness of the shell layer due to the fact that the technique is based on self-terminated surface reactions.[41-43] Moreover, ALD can develop reproducible, homogenous and conformal coatings on the surface of high-aspect ratio nanostructured substrates at low temperatures while preserving the fundamental properties of the core materials.[44-46] The gas-sensing properties of the as-synthesized SnO_2-SiO_2/*N* CSNWs are studied as a function of the SiO_2-shell thickness allowing to elucidate the underlying gas-sensing mechanism and to propose clear structure–property correlations. To the best of our knowledge, this is the first report where the role of the amorphous SiO_2 shell layer conformally coated onto 1D SnO_2 nanostructures has been studied by designing structurally well-defined hierarchical heterostructures with varying thickness of the shell layer.

Materials and Methods

(3-Aminopropyl)triethoxysilane, (APTES, $(H_2N(CH_2)_3Si(OC_2H_5)_3$, 99%) and SnO_2 (99.9%) were purchased from Sigma-Aldrich. Ozone (O_3) was generated using pure oxygen (99.99%) in a BMT803N ozone generator. Argon, nitrogen, and oxygen were purchased from Air Liquide (99.99% purity), and all other certified gases for sensing tests were supplied by the SOL Group (Italy). All chemicals and reagents were of analytical grade and used without further purification unless otherwise stated.

Substrate Preparation and Growth of SnO_2 Nanowires

The comprehensive of the substrate preparation is reported in our earlier reports.[8,47] Briefly, an ultrathin layer of Au catalyst was deposited (onto the pre-cleaned alumina substrate, 2×2 mm^2) using magnetron sputtering (Kenotec Sputtering system, Italy) at 7 sccm of argon using a RF power of 50 W at a pressure of 5×10^{-3} mbar, for 5 s. SnO_2 NWs were produced directly onto the Au-catalysed alumina substrates by VLS deposition in a custom designed tubular furnace (by Lenton) using SnO_2 powder as a source material. SnO_2 powder and Au catalysed substrates contained in alumina crucibles were placed inside the alumina tube. The powder was placed in a relatively high-temperature region and heated up to the 1370 °C leading to its evaporation. Alumina substrates were placed in a comparatively colder region (860 °C) to promote the condensation of evaporated

material. Argon gas, at 100 sccm mass flow, was used as the carrier gas to transport the vapors of the SnO_2 source material to the Au-catalyst supported onto alumina, where the deposition time was set to 2 min while maintaining the total pressure inside the tube at 100 mbar.

Synthesis of SnO_2-SiO_2 Core–Shell Nanowires (CSNWs)

SiO_2-shell layer was directly deposited onto the SnO_2 nanowires (NWs) grown onto the alumina substrate after the contacts were already deposited (**see below and Figure 1**). The surfaces of the platinum contacts were masked using a custom-designed copper frame shadow masked. Pre-cleaned silicon-wafers (Siegert wafer B014002, cleaned in piranha solution) were also put in the ALD chamber along with the SnO_2 nanowires samples to calibrate the thickness of the SiO_2 thin film by spectroscopic ellipsometry (SE). Atomic layer deposition (ALD) was performed in commercial ALD systems by Arradiance. The ALD systems were evacuated (*ca.* 8.5×10^{-3} mbar), and the temperature of the ALD chamber was stabilized at 160 °C before starting the ALD process. Prior to the ALD, all the samples were in situ treated with UV-ozone to remove organic impurities, if any (total exposure time, 300 s). The temperature of the reaction chamber and the supply lines was maintained at 160 and 120 °C, respectively. (3-Aminopropyl)triethoxysilane (APTES) kept at 80 °C was used as Si precursor, whereas millipore water and ozone (kept at RT) were used as oxygen sources.[48] APTES, H_2O and O_3 were introduced into the reaction chamber in a sequential manner using argon both as carrier and as purging gas. One ALD cycle was adjusted as a sequence of 2 s pulse of APTES, 30 s exposure, 30 s Ar purge, 0.2 s H_2O pulse, 30 s exposure, 40 s Ar purge, 0.2 s O_3 pulse, 30 s exposure, and 40 s of Ar purge. The thickness of the SiO_2 film was controlled by varying the number of ALD cycles (20–130). The samples are named as SnO_2-SiO_2/*N*, where *N* stands for the number of SiO_2 ALD cycles (i.e., 20, 40, 60, 90 and 130 ALD).

Morphological and Microstructural Characterization

The thickness of the SiO_2 film was initially estimated on silicon wafers by using a spectroscopic ellipsometer from Sentech. The data was collected at an incident angle of 70° for wavelengths ranging from 370 to 1000 nm and an average of at least three measurements were considered. High-resolution transmission electron microscopy (HRTEM), high-angle annular dark-field scanning transmission electron microscopy (HAADF-STEM) selected area electron diffraction (SAED) and energy-dispersive X-ray spectroscopy (EDX's) elemental mapping were performed using a FEI Talos F200S scanning/transmission electron microscope (S/TEM) operated at 200 kV. The TEM data including the SiO_2-shell thickness estimation directly onto the SnO_2 NWs were performed using Velox^{TM} analytical software. Scanning electron microscopy (SEM) images were acquired with a FEI Quanta 200 FEG microscope.

Sensing Device Fabrication and Measurement Setup

Six different batches of gas-sensing devices were fabricated including the pristine SnO_2 NWs and SnO_2-SiO_2/*N* CSNWs with varying thicknesses of the SiO_2-shell layer (i.e., 1.8–10.5 nm). Prior to the SiO_2 ALD, two parallel contacts were deposited on the alumina substrate by a two-step deposition process. TiW alloy adhesion layers (as pads) and Pt electrodes (thickness, ~1 μm) were deposited by dc magnetron sputtering (70 W argon plasma, RT, *ca.* 0.55 Pa) with a deposition time of 3 and 20 minutes, respectively. A micro-patterned platinum heater was also deposited on the backside of alumina substrate using the same two-step process. Finally, all of the devices were mounted on the TO packages using electro-soldered gold wires. The material synthesis and device fabrication process is schematically described in **Figure 1**.
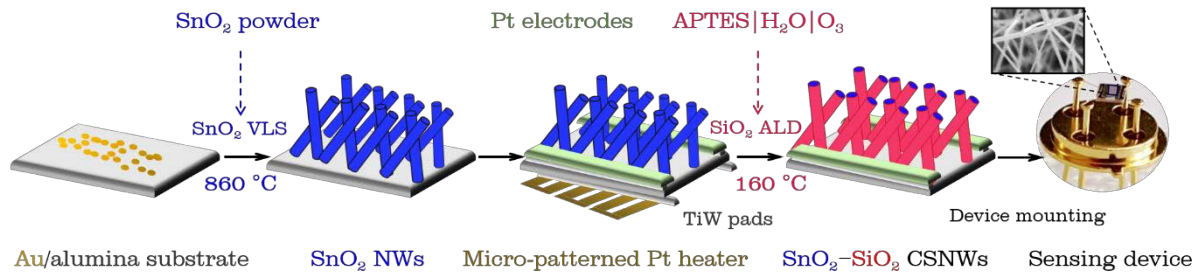
Figure 1. Schematics of the synthesis of SnO_2-SiO_2/*N* CSNWs and the device fabrication for gas-sensing measurements.

Gas-sensing measurements

A flow-through technique was used to analyze the sensing response of the fabricated devices in a homemade stainless steel chamber (volume, 1 dm^3) that is placed inside a climate chamber set at 20 °C (Angelantoni MTC 120, Italy). The temperature of the sensors was controlled independently by using a Thurlbly-Thandar PL330DP power supply. All the sensors were thermally stabilized at the set temperature for 8 hours prior to the measurement in the presence of 0% and 40% relative humidity (RH% at 20 °C).

Test gases with certified concentrations and dry air were mixed using mass flow controllers (MKS, Germany), where the total mass flow was maintained as 200 sccm. After the 30 minutes of exposure to a fixed concentration of the analyte-gas, synthetic airflow was restored for 60 minutes to allow a baseline recovery. A fixed voltage of 1 V was applied to the sensors (Agilent E3631A power supply) and the conductance of each sensor was measured continuously by using a picoammetters (Keithley 486, USA) in different atmospheres and temperatures. The sensors response was determined by the variation in resistance/conductance using the equation (1) and (2) for oxidizing and reducing gases, respectively.

$$\text{Response } (S) = \frac{G_{\text{air}} - G_{\text{gas}}}{G_{\text{gas}}} = \frac{\Delta G}{G_{\text{gas}}} \qquad (1)$$

$$\text{Response } (S) = \frac{G_{\text{gas}} - G_{\text{air}}}{G_{\text{air}}} = \frac{\Delta G}{G_{\text{air}}} \qquad (2)$$

Where G_{air} and G_{gas} are the sensor conductance in the synthetic air and the target gas flows, respectively. Gas-sensing characteristics were studied for various concentrations of hydrogen and some common interfering gases, i.e.*,* ethanol, acetone, carbon monoxide, hydrogen sulfide and NO_2. Initially, to find the optimal working temperature for all the sets of sensing devices a temperature screening was performed between 200–500 °C. After the sensing parameters have been studied, the experimental data for calibration (response as a function of hydrogen concentration) at optimal working temperature were fitted to the power-law trend (**equation 3**).

$$\text{Response} = A \, [\text{Gas concentration}]^B \qquad (3)$$

where *A* and *B* are constants related to the material composition and stoichiometry of the surface chemical reactions, respectively.[8,47]

<u>**Results and Discussion**</u>

Structural Characterization

Figure S1a shows bright-field (BF) TEM image for an overview of non-coated SnO_2 NWs. It can be seen that as-synthesized SnO_2 NWs are relatively homogeneous showing nanowires like morphology with diameters ranging from 50–70 nm. Moreover, SEM micrographs (for bare SnO_2 NWs and SnO_2-SiO_2/130 CSNWs) in **Figure S1b–d** further confirmed that the pristine SnO_2 NWs are identical in their size and diameter, and homogeneously dispersed onto the alumina substrate. After the ALD process, the SEM images showed a well-preserved SnO_2 morphology.

An insight into the morphology and microstructure of all the synthesized samples was investigated by high-resolution transmission electron microscopy (HRTEM). BF-HRTEM image for an isolated pristine SnO_2 nanowire is shown in **Figure 2a**. The corresponding SAED pattern (**Figure 2b**) shows reflections corresponding to a single crystal of cassiterite (rutile-type structure) aligned along the $[\bar{1}00]$ zone axis, where the corresponding reflections are marked accordingly (ICDD 00-001-0625). The BF-TEM micrographs of isolated SiO_2-coated SnO_2 NWs (SnO_2-SiO_2/N) and their magnified images (*cf.* insets) show that SnO_2 nanowires are homogeneously and conformally coated with a continuous film of SiO_2 confirming the hierarchical core-shell like heterostructure (**Figure 2c–h**). It can be seen that the thicknesses of the SiO_2 shell layer onto the SnO_2 nanowires are calibrated and increased with increasing the number of SiO_2 ALD cycles. The average thickness of the SiO_2 film measured from the TEM images are 1.8, 3.1, 4.8, 7.5 and 10.5 nm for 20, 40, 60, 90 and 130 ALD cycles, respectively (**Table S1**). The plot of the thickness of SiO_2 *vs* the number of ALD cycles shows a good linearity (R^2 = 0.998) with a slope corresponding to a growth per cycles (GPC) as 0.81 Å/cycle. The thicknesses of the SiO_2 coatings as a function of the ALD cycles estimated from the TEM images and by the ellipsometry are comparable, proving the saturation behaviour for the ALD process on both substrates (**Table S1 and Figure S2**). **Figure 2i** shows SAED pattern corresponding to an isolated SnO_2-SiO_2/130 CSNW in **Figure 2h**, which shows a single crystalline pattern for SnO_2, where the corresponding reflections marked correspond to $[\bar{1}\bar{1}3]$ zone axis. Notably, other than the cassiterite phase of SnO_2, no additional reflections are present that can be indexed to ALD-deposited SiO_2. This shows that SnO_2 remained single crystalline after SiO_2 ALD, while the ALD-deposited SiO_2 thin film is as expected amorphous.[44] The magnified view in the inset in **Figure 2g** clearly demonstrates the presence of two distinctive phases, i.e., crystalline SnO_2–core and amorphous SiO_2–shell. The calculated *d*-spacing as 0.335 nm in SnO_2 region can be indexed to the (110) plane of SnO_2 cassiterite phase (**Figure 2g**).

The high-angle annular dark-field scanning transmission electron microscopy (HAADF-STEM) images for the SnO_2-SiO_2/N (N, 60 and 90) samples show a uniform and conformal coverage of the SnO_2 nanowires with an amorphous SiO_2 thin film. This is consistent with the bright-field TEM images, where the phases of SnO_2 and SiO_2 can be identified easily due to their different *Z*-contrast (**Figure 2j,k**). The corresponding energy-dispersive spectroscopy (EDX) images for the elemental mappings show the presence of Si, Sn, and O atoms with a homogenous and conformal SiO_2 film onto the SnO_2 nanowires further confirming the CSNW-like heterostructures (**Figure 2j,k**). **Figure S3** shows the EDX spectra corresponding to the elemental mappings shown in **Figure 2j,k** for the SnO_2-SiO_2/60 and SnO_2-SiO_2/90 CSNWs.
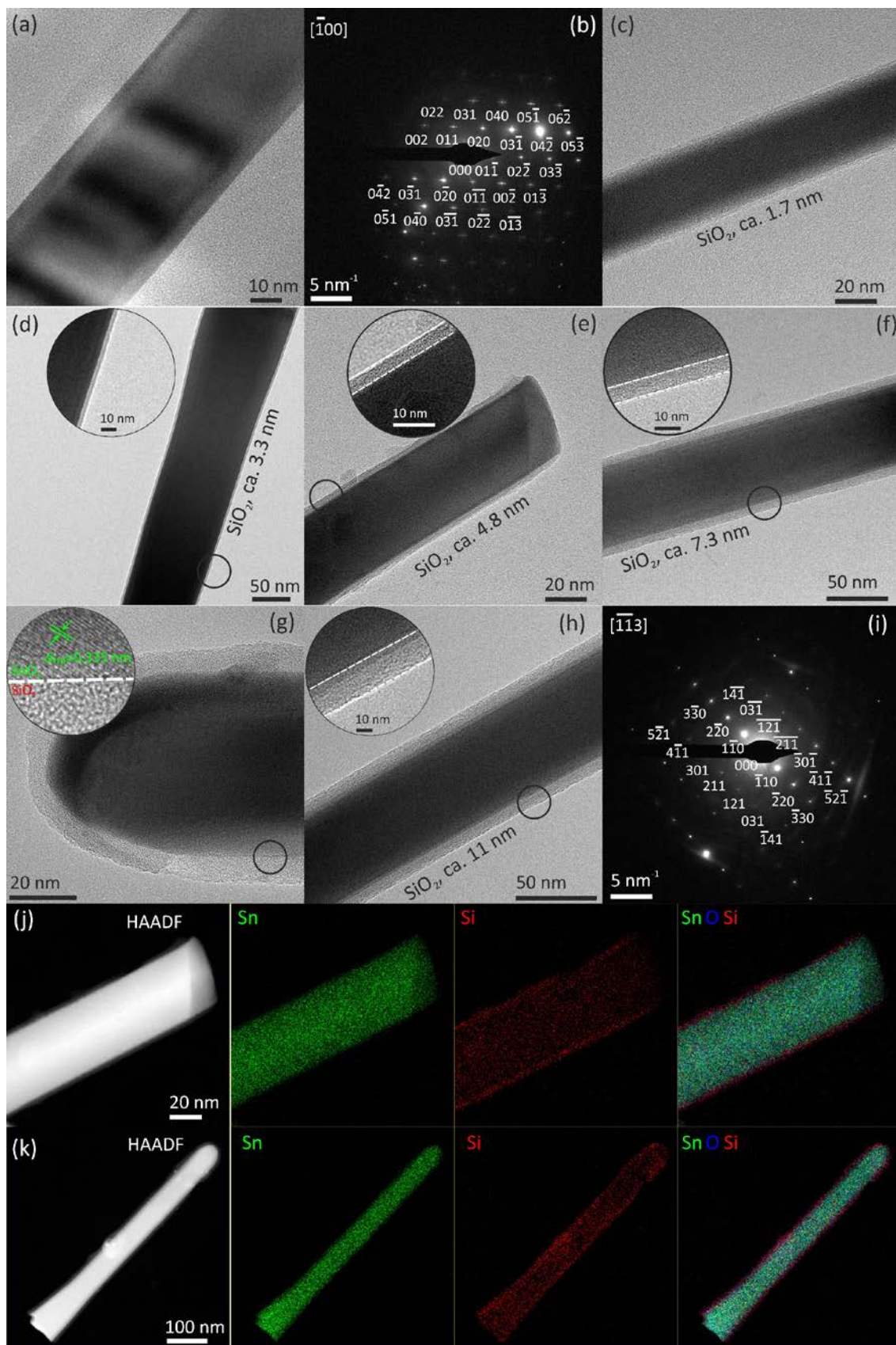
Figure 2. Bright-field transmission electron microscopy (TEM) micrographs of pristine SnO$_2$: (a) an isolated SnO$_2$ nanowire and (b) the corresponding SAED pattern. BF-TEM images for the isolated SnO$_2$-SiO$_2$/*N* CSNWs: (c) SnO$_2$-SiO$_2$/20, (d) SnO$_2$-SiO$_2$/40, (e) SnO$_2$-SiO$_2$/60, (f, g) SnO$_2$-SiO$_2$/90, (h) SnO$_2$-SiO$_2$/130 and (i) Corresponding SAED pattern. HAADF-STEM images and the corresponding EDX

elemental mappings for the (j) SnO_2-SiO_2/60 and (k) SnO_2-SiO_2/90 CSNWs. The insets in d–h show magnified view of the encircled areas in the corresponding micrographs.

Electrical Characteristics

To study the electrical behaviour of the sensing devices and to see if there is a significant effect on the electrical conductance due to the interface at SnO_2-base material and the SiO_2-shell, the baseline conductance of all of the pristine SnO_2 NWs and SiO_2-coated SnO_2 CSNWs samples were recorded in nitrogen and in air. **Figure S4** shows the baseline conductance of all the fabricated devices as a function of temperature (RT–500 °C) under nitrogen. All the sensors show a monotonic increase in conductance with increasing the temperature from RT to 500 °C, thereby confirming a dominant semiconducting behaviour of the CSNWs heterostructures.[16] Thus, the insulating nature of the SiO_2-shell layers did not alter the semiconducting conductance-temperature behaviour of SnO_2 NWs. Noticeably, in our sensing-devices because the SnO_2 NWs are contacted before the SiO_2 deposition, *i.e.* the electrodes are connected to the SnO_2-core network directly, the insulating SiO_2-coating acts only as a surface modifier of the already prepared device. However, a finite SiO_2-loading effect was observed in which the electrical conductance decreased for all of the SnO_2-SiO_2/*N* CSNWs sensors as compared to the pristine SnO_2 NWs. Under nitrogen, it can be assumed that the acceptor states due to the chemisorption effect of oxygen species are negligible. Therefore, a drastic decrease in electrical conductance (or increase in resistance) would point to an electron-depletion-layer (EDL) at the interface of SnO_2-core and SiO_2-shell layer similar to that has been demonstrated in the case of electronic coupling between SMOX-SMOX interfaces.[49-50] It can be seen that conductance of SnO_2 NWs samples decrease significantly (up to four orders of magnitude) depending on the thickness of the SiO_2 coating at a particular operating temperature (**Figure S4**). This is attributed to the additional component of the resistance due to the extraction of electrons from SnO_2 NWs conduction band by SiO_2.[51] Thus, a junction is formed at the SiO_2–SnO_2 interface,[29,52-54] which introduced an electron-depletion-layer (EDL) at the SnO_2 near surfaces (**Figure 4d**).

In addition, the electrical conductance of all the sensors were recorded (in dry air) and these values were used as reference and baseline for the gas-sensing study. There is a clear difference in the baseline conductance (G_{air}) among pristine and SiO_2-coated SnO_2 NWs sensors (**Figure 3a**). As a matter of fact, the conductance of the SnO_2-SiO_2 CSNWs sensors in air decreased sharply with the increase of the SiO_2-shell thickness up to the *ca.* 4.8 nm. It is well known that the electrical conductance at a particular temperature is seriously affected by the concentration of absorbed oxygen species.[8,50] A comparison of the baseline conductance of all of the pristine and SiO_2-coated SnO_2 NWs sensors in nitrogen to the same sensor in dry air shows that the conductance decreased with the introduction of dry air (baseline conductance values, **Figure 3a**). This shows that oxygen can diffuse through the SiO_2-shell to the SnO_2 NWs. On the other hand, the extent of difference in conductance from nitrogen to dry air decreased for the samples with higher thickness (> 4.8 nm), manifesting that thicker SiO_2-shell film hinder the diffusion of oxygen species to the SnO_2 surfaces (**Figure 3a**). Likewise, the baseline-conductance of the SnO_2/SiO_2-*N* CSNWs sensors show a steep-declined with increasing the SiO_2-shell layer thickness up to the thickness *ca.* 4.8 nm (SnO_2-SiO_2/60 CSNWs), and then it stayed at a similar value with further increasing the shell thicknesses (studied up to *ca.* 10.5 nm). At higher thicknesses, the thick SiO_2-shell film impedes the diffusion of oxygen species to the SnO_2 NWs surfaces.

Gas Sensing Properties

The gas-sensing tests were performed for a series of SnO$_2$ NWs and SnO$_2$-SiO$_2$/N CSNWs devices in the presence of hydrogen and common interfering gases (namely; ethanol, acetone, CO and H$_2$S) at different working temperatures in dry air (0% RH) and in a relative humid environment (40% RH). The isothermal electrical conductance transients toward various concentrations of H$_2$ (50, 200, and 500 ppm) at 500 °C in dry air (RH 0%) and 40% of relative humidity (RH 40%) are presented in **Figure 3b,c** and **Figure S5a**. It can be seen that as the hydrogen gas was introduced into the testing chamber, the electrical conductance of all the sensors increased, and shortly reached a maximum conductance value, followed by a recovery to their baseline as the hydrogen exposure was stopped (**Figure 3b**). This shows a typical n-type response of the SnO$_2$-based SMOX gas-sensors. SnO$_2$ is a well-known non-stoichiometric SMOX showing n-type semiconducting behaviour due to the presence of oxygen vacancies.[8] As described earlier (*cf.* electrical characteristics section), the presence of SiO$_2$-shell did not influence the semiconducting behaviour (n-type) of the SnO$_2$ NWs. Thus, the SnO$_2$-SiO$_2$/N CSNWs devices show a response due to the SnO$_2$–core in the CSNWs heterostructures and the electrons conduction path should be mainly confined to the SnO$_2$-core, *i.e.* along the conductive core-axis (*cf.* discussion below). Moreover, all the sensors show a dynamic reversible response, where the response towards H$_2$ increases with increasing the concentration in both dry air and in air with 40% RH (**Figure 3b,c**).

Figure 3d represents the sensing-response of the devices fabricated with SnO$_2$ NWs and SnO$_2$-SiO$_2$/N CSNWs with varying thicknesses of the SiO$_2$-shell layer toward H$_2$ (200 ppm) in the temperature range of 200–500 °C. It can be seen that the response of all of the sensors increased with increasing the temperature and all of the SnO$_2$-SiO$_2$/N CSNWs sensing devices show the highest response towards hydrogen at 500 °C. This is due to the high diffusion rate of H$_2$ molecules at this higher temperature, and comparatively higher thermal energy to overcome the activation energy barrier for the surface reactions and enhancing the diffusion of the molecules to the SnO$_2$ surface across the SiO$_2$ coating.[55] The sensing response of the different sensors as a function of H$_2$ concentration at their optimal working temperature (500 °C) in dry air (0% RH) are shown in **Figure 3e**. Higher the concentration of hydrogen, the greater is the response of the sensors. The calibration curves, response *vs* concentration follow a typical power-law relation (in agreement with the **eq 3**) for SMOX-sensors, further confirming the absence of any saturation process.[8,37] The sensors detection limit is calculated while considering the minimum response value of 1 in **eq 3**. The values of different parameters calculated by the power-law fits are summarised in **Table S2**. The best performing sensors show a detection-limit at ppb-level (0.094 and 0.082 ppm for SnO$_2$-SiO$_2$/40 and SnO$_2$-SiO$_2$/60 CSNWs sensors, respectively) at 500 °C. Moreover, the SnO$_2$-SiO$_2$/60 CSNWs sensor shows a lower detection limit for hydrogen (0.082 ppm) as compared to ethanol (2.3 ppm) and acetone (3.5 ppm), *cf.* **Figure 3f** and **Table S3**. It is of note that SnO$_2$-SiO$_2$/N CSNWs sensors showed a good selectivity towards hydrogen together with a comparatively higher sensing-response as compared to the pristine SnO$_2$ NWs both in dry air and in air with 40% RH. The response of all the fabricated sensors decreased with increasing the relative humidity (**Figure S5b**). This reduction of the gas-sensing response in humid environment for SMOX-based gas sensors is due to the competition of adsorption between the analyte gas and the water molecules as reported earlier.[8,37] **Figure 3g** and **Figure S5b** compare the sensing response for the pristine SnO$_2$ NWs and SnO$_2$-SiO$_2$ CSNWs with different thickness of the SiO$_2$-shell layer, in dry air and in 40% RH, respectively. The SnO$_2$-SiO$_2$ CSNWs sensors with a shell thickness approx. 1.8–4.8 nm show an enhanced sensitivity toward H$_2$ as compared to the pristine SnO$_2$ NWs sensors. Indeed, SnO$_2$-SiO$_2$/60 CSNWs sensor shows a 6 to 7-folds increase in response as compared to the pristine SnO$_2$ NWs for all of the tested

concentrations of hydrogen (50–500 ppm) at 500 °C *cf.* **Figure 3g**. In addition, among the SnO_2-SiO_2/N CSNWs sensors, the sensing-response increased initially with increasing the SiO_2-shell thickness up-to the *ca.* 4.8 nm (*i.e.*, for SnO_2-SiO_2/60 CSNWs), and then it decreased with further increasing the SiO_2-shell thickness. For example, the pristine SnO_2 NWs, and SnO_2-SiO_2/N CSNWs sensors with 20, 40, 60, 90 and 130 ALD cycles show a response of 7, 13, 25, 42, 6 and 3 towards 50 ppm of hydrogen, respectively (**Figure 3g**). The sensor fabricated with SnO_2-SiO_2/60 CSNWs shows the best response among all the fabricated sensors. This sensor revealed a distinguished response of 160 toward 500 ppm of H_2 (a concentration that is still two-orders-of-magnitude lower than the explosive limit of H_2) at 500 °C in dry air.

Figure 3h shows the sensing response of the pristine SnO_2 NWs and SnO_2-SiO_2/N CSNWs toward hydrogen and other interfering gases at the optimal working temperature of 500 °C. The response towards H_2 greatly increases after SiO_2 coating. On the other hand, the response to the acetone, ethanol, CO and H_2S is less significant and it is almost not affected by the SiO_2 coating. The SnO_2-SiO_2/60 CSNWs, the best performing sensor, show a response of 6.2, 3.8, 4, 1 and 42 toward ethanol (50 ppm), acetone (50 ppm), CO (100 ppm), H_2S (20 ppm) and hydrogen (50 ppm), respectively (**Figure 3h**). Clearly, the SnO_2-SiO_2/N CSNWs sensors exhibit a negligible cross-sensitivity to the selected interfering gases making them appropriate for real time hydrogen-detection applications. A comparison of our sensors to some state-of-the-art SnO_2-based nanostructures for the selective detection of hydrogen is summarized in **Table S4**. Indeed, the present study clearly demonstrates the transduction mechanism towards hydrogen sensing of structurally well-defined 1D core-shell nanowires with a well-defined SiO_2 shell thickness allowing to propose clear structure-property correlations.
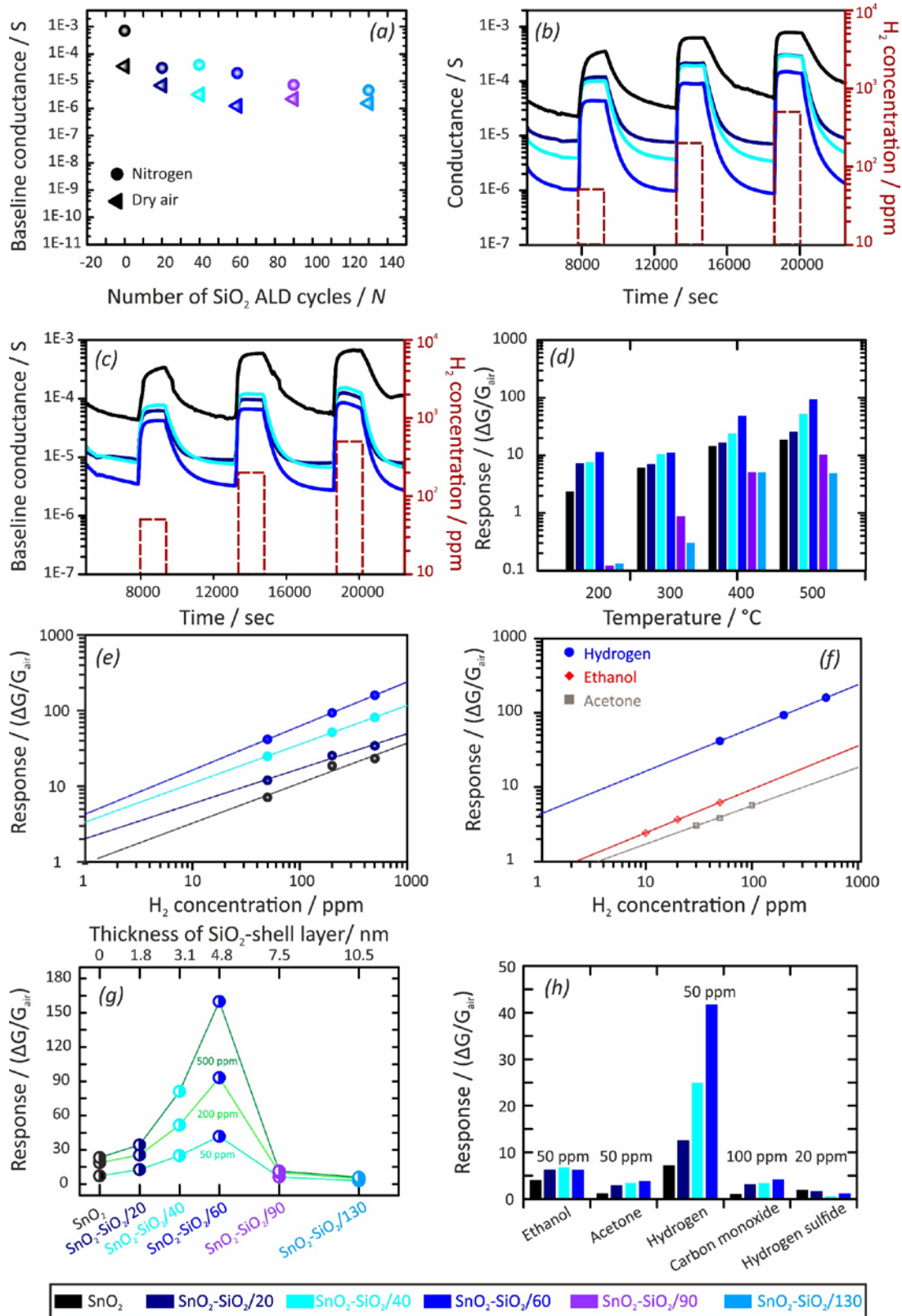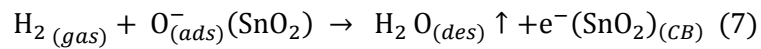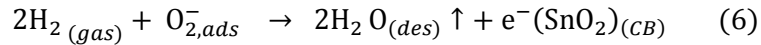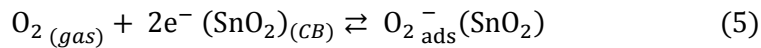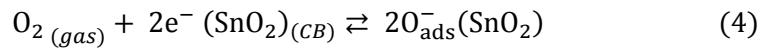
Figure 3. (a) Baseline electrical conductance of SnO$_2$ NWs and the SnO$_2$-SiO$_2$/N CSNWs sensors devices in dry air and in nitrogen at 500 °C. Dynamic response of the sensors fabricated with bare SnO$_2$ NWs and the SnO$_2$-SiO$_2$/N CSNWs at 500 °C to the different concentrations of H$_2$ (50–500 ppm), (b) in dry air and (c) in air with 40% RH. (d) The response of the bare SnO$_2$ NWs and the SnO$_2$-SiO$_2$/N CSNWs sensors toward 200 ppm of H$_2$ at different temperatures (200–500 °C). The power-law fits of the (e) sensing-response vs different concentrations of hydrogen at 500 °C for the sensors

fabricated with pristine SnO$_2$ NWs and various SnO$_2$/NiO-X CSNWs heterostructures in dry air, and (f) sensing-response vs different concentrations of hydrogen, acetone and ethanol for the best performing sensor (SnO$_2$-SiO$_2$/60 CSNWs) at optimal working temperature of 500 °C. (g) The response of the bare SnO$_2$ NWs and the SnO$_2$-SiO$_2$/N CSNWs sensors with varying thicknesses of the SiO$_2$ amorphous shell layer to hydrogen (50, 200 and 500 ppm) at 500 °C. (h) Response of the bare SnO$_2$ NWs and the SnO$_2$-SiO$_2$/N CSNWs sensors to the hydrogen (50 ppm) and common interfering gases, i.e., acetone (50 ppm), ethanol (50 ppm), and carbon monoxide (100 ppm) and hydrogen sulfide (20 ppm) at 500 °C, demonstrating a good selectivity towards hydrogen. Legends for all the panels are same as shown at the bottom of the Figure.

Gas Sensing Mechanism and Discussion

Figure 4 shows the schematics of the regions involved in the transduction mechanism for both the SnO$_2$ NWs and the SnO$_2$-SiO$_2$/N CSNWs heterostructures. A detailed sensing mechanism for SnO$_2$ NWs has already been described in our earlier report [8]. Briefly, the sensor signal is based on the charge transfer as a result of redox reactions between the chemisorbed oxygen species (i.e., O^{2-}, O$_2^-$, and O$^-$) and the analytes at the surfaces of the SMOX, which mainly induce a change in the electrical resistance of the device. In air, oxygen species adsorbed onto the SnO$_2$ surfaces withdraw electrons from the conduction band of the SMOX resulting in an electron depletion layer (EDL) in the near surfaces (**eq. 4,5**). This creates a surface potential, *i.e.* a Schottky barrier at the surface, resulting in an upward band bending. Another potential barrier is created in case of a SnO$_2$ NWs network due to the contacts between the depleted surfaces of the nanowires with each other (back-to-back Schottky barrier) at the SnO$_2$–SnO$_2$ homojunction (**Figure 4a,b**).[37-38,56]

When an analyte such as hydrogen (a reducing-gas) is introduced, it is oxidized during the reaction with the adsorbed oxygen species at the SnO$_2$ surface by donating electrons back to the conduction band of the SnO$_2$ NWs, thus accordingly narrowing the electron depletion region (decreasing the potential barrier height), **eq. 6,7**. This results in an increase in the width of the conduction channel and therefore to an increase of the conductance of the sensor (**Figure 4c**). Hence, the change in resistance of the device fabricated with pristine SnO$_2$ NWs is a combination of a series of resistance, *i.e.* change of the surface depletion region and the potential barrier height due to back-to-back SnO$_2$-SnO$_2$ homojunction.[16,57] Importantly, due to the small size and diameter of the SnO$_2$ NWs, these changes in the electrical signals become greater, where the space-charge region participates significantly along with the potential barrier at back-to-back homojunction.[8,16,58]

$$O_{2\,(gas)} + 2e^- \,(SnO_2)_{(CB)} \rightleftarrows 2O_{ads}^-(SnO_2) \qquad (4)$$

$$O_{2\,(gas)} + 2e^- \,(SnO_2)_{(CB)} \rightleftarrows O_{2\,ads}^-(SnO_2) \qquad (5)$$

$$2H_{2\,(gas)} + O_{2,ads}^- \;\rightarrow\; 2H_2O_{(des)}\uparrow + e^-(SnO_2)_{(CB)} \qquad (6)$$

$$H_{2\,(gas)} + O_{(ads)}^-(SnO_2) \;\rightarrow\; H_2O_{(des)}\uparrow + e^-(SnO_2)_{(CB)} \quad (7)$$

In the SiO$_2$ coated SnO$_2$ CSNWs, an additional heterojunction is introduced between the SiO$_2$-shell and the SnO$_2$-core, thereby narrowing the conduction channel along the SnO$_2$-core and increasing the resistance of the whole system.[51-54] Importantly, the electrons conduction path should be mainly confined to the SnO$_2$-core, *i.e.* along the conductive core-axis (**Figure 4d**).[8]

When the SnO$_2$-SiO$_2$ CSNWs sensor is exposed to air, oxygen can diffuse through the SiO$_2$-shell to the SnO$_2$ core and chemisorbs by capturing electrons from the conduction band of the SnO$_2$ (*n*-type

SMOX). Thus the width of the EDL increases when the sensor is exposed to air narrowing the conduction channel (**Figure 4e**). The SiO$_2$–shell acts as a molecular sieve where the analyte has to diffuse through the SiO$_2$ layer to react at the SnO$_2$ surface. Therefore, the density of the films, thickness and the presence of pinholes/pores in the SiO$_2$-shell can critically affect the selectivity and sensitivity of the sensor.[19,25,30] These aspects control the diffusion of gas molecules with respect to their size and nature, such as due to its smaller size (for example the molecular diameters of gases H$_2$, H$_2$O, O$_2$, CO are reported as 2.18, 2.72, 2.96 and 3.80 Å, respectively)[27] hydrogen can diffuse through the shell layer easier than the other analytes of interest.[59] Therefore, the diffusion of comparatively large-sized gases such as acetone, ethanol, carbon monoxide and hydrogen sulfide became negligible.[19] Thus, the SiO$_2$-shell layer deposited on top of the SnO$_2$ NWs is mainly responsible for the selectivity towards hydrogen. Hydrogen (a reducing gas) is oxidized to water when it reacts with adsorbed oxygen species at the SnO$_2$ surface, accordingly narrowing the electron depletion region, **eq. 6,7**. This results in an increase in the width of the conduction channel and accordingly the conductance of the sensor increases (**Figure 4f**). The higher sensing-response of SnO$_2$-SiO$_2$/20–60 CSNWs sensors as compared to the bare SnO$_2$ NWs is due to the greater width and a comparatively more resistive electron-depletion-layer.[29,37,51] Indeed, this highly resistive EDL increased the tendency of electron acceptance from hydrogen.[16,29,37] However, with the increase of the shell thickness beyond the critical thickness (4.8 nm, in this study, *cf.* **Figure 2g**), the SiO$_2$ layer became too thick to diffuse the hydrogen to the sensing layer and its oxidation products out, thereby it decreased the sensor response (*cf.* the sensitivity of the SnO$_2$-SiO$_2$ /90 and SnO$_2$-SiO$_2$/130 CSNWs sensors in **Figure 3g**).[25]
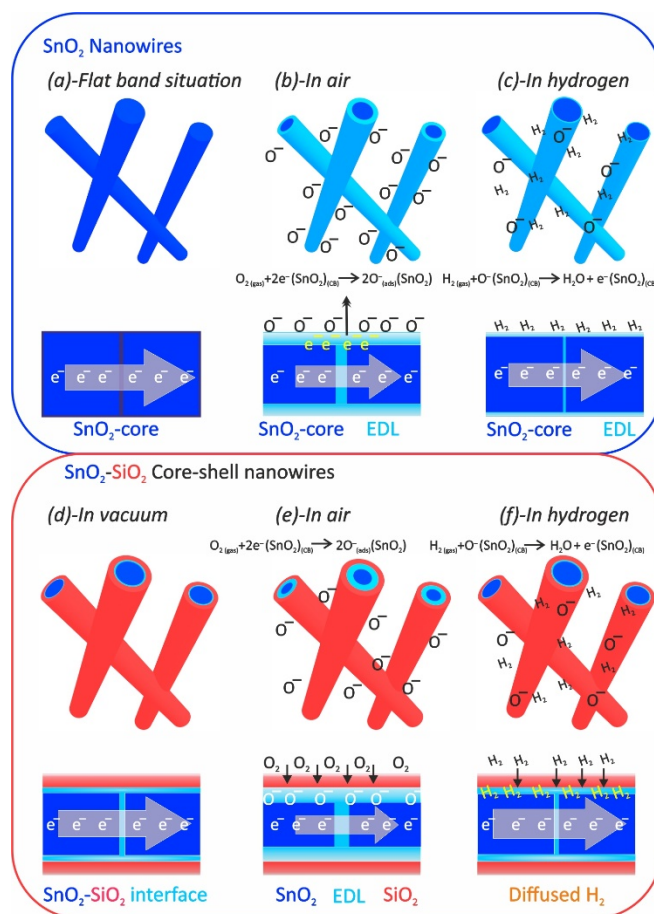

Figure 4. Schematics of the sensing mechanism and effective conduction channel for the pristine SnO$_2$ NWs and SnO$_2$-SiO$_2$ CSNWs heterostructures. (a–c) represents pristine SnO$_2$ NWs; (a) in vacuum

(flat-band situation), (b) in air, the chemisorbed oxygen species withdrawing electrons from the conduction band, creating an electron depletion layer, thus narrowing the conduction channel and enhancing the barrier height at the surface and at the back-to-back contacts, (c) in H_2, the hydrogen adsorbed onto the SnO_2 surface donating electrons back to the depleted surfaces, reducing the barrier height along with expanding the conduction channel. (d–f) SnO_2-SiO_2 CSNWs; (d) in vacuum, where a SiO_2-SnO_2 junction is formed by creating the electron-depletion-layer (EDL) at the interface of the two materials (indeed the conduction channel became narrow as compared to the pristine SnO_2 NWs), (e) in air, as the chemisorbed oxygen species withdraw electrons from the conduction band of SnO_2, thus broadening the EDL at the interface with further narrowing the charge conduction channel, (f) in hydrogen, amorphous SiO_2-shell layer acts as a selective filter for hydrogen, the hydrogen species can diffuse at the SnO_2 surface and oxidize releasing electrons back to the conduction band of SnO_2, thus narrowing the EDL and broadening of the conduction channel.

Conclusion

In this article, we have studied the gas-sensing properties and the underlying transduction mechanism of well-defined SnO_2-SiO_2 core-shell nanowires heterostructures with varying thickness of the amorphous SiO_2-shell layer (1.8–10.5 nm in thicknesses). The selectivity and response of pristine SnO_2 sensors are greatly enhanced by a conformal and homogeneous SiO_2 coating. The electrical properties and the sensor response of the SnO_2-SiO_2 CSNWs heterostructures strongly depend on the thickness of the SiO_2 shell layer. The SnO_2-SiO_2/60 CSNWs sensor with a shell layer thickness of 4.8 nm showed an optimized response of 160 (*ca.* 7-folds higher than pristine SnO_2 NWs) toward 500 ppm of hydrogen at 500 °C along with a lower detection-limit at ppb-level (0.082 ppm). This is attributed to an increase of the width of the electron-depletion-layer due to a strong core-shell coupling, where the conduction pathway is strictly confined to the SnO_2 core. In addition, an enhanced selectivity towards hydrogen is demonstrated due to a "masking effect" of the SiO_2 shell allowing hydrogen to more easily diffuse to the SnO_2 NWs surface compared to other reducing gases such as ethanol and carbon monoxide. The outstanding sensing properties of the SnO_2-SiO_2/*N* CSNWs can therefore be attributed to our heterostructured materials presenting at the same time a high surface area, a homogeneous and conformal, and electronically coupled SiO_2 shell layer presenting an optimized thickness. All in all, because our study precisely correlates the structural characteristics of well-defined SnO_2-SiO_2 heterostructures to the gas-sensing properties, we anticipate that it will be helpful for the understanding and the application of next-generation gas-sensing material.

References

1. Liu, Y.; Parisi, J.; Sun, X.; Lei, Y., Solid-state gas sensors for high temperature applications – a review. *J. Mater. Chem. A* **2014,** *2* (26), 9919-9943.
2. Russo, P. A.; Donato, N.; Leonardi, S. G.; Baek, S.; Conte, D. E.; Neri, G.; Pinna, N., Room-Temperature Hydrogen Sensing with Heteronanostructures Based on Reduced Graphene Oxide and Tin Oxide. *Angew. Chem. Int. Ed.* **2012,** *51* (44), 11053-11057.

3.   Hübert, T.; Boon-Brett, L.; Black, G.; Banach, U., Hydrogen sensors – A review. *Sens. Actuators, B* **2011,** *157* (2), 329-352.

4.   Kim, S. M.; Kim, H. J.; Jung, H. J.; Park, J.-Y.; Seok, T. J.; Choa, Y.-H.; Park, T. J.; Lee, S. W., High-Performance, Transparent Thin Film Hydrogen Gas Sensor Using 2D Electron Gas at Interface of Oxide Thin Film Heterostructure Grown by Atomic Layer Deposition. *Adv. Funct. Mater.* **2019,** *29* (7), 1807760.

5.   Penner, R. M., A Nose for Hydrogen Gas: Fast, Sensitive H2 Sensors Using Electrodeposited Nanomaterials. *Acc. Chem. Res.* **2017,** *50* (8), 1902-1910.

6.   Sberveglieri, G.; Baratto, C.; Comini, E.; Faglia, G.; Ferroni, M.; Pardo, M.; Ponzoni, A.; Vomiero, A., Semiconducting tin oxide nanowires and thin films for Chemical Warfare Agents detection. *Thin Solid Films* **2009,** *517* (22), 6156-6160.

7.   Sitarz, M.; Kwoka, M.; Comini, E.; Zappa, D.; Szuber, J., Surface chemistry of SnO2 nanowires on Ag-catalyst-covered Si substrate studied using XPS and TDS methods. *Nanoscale Res. Lett.* **2014,** *9* (1), 43.

8.   Raza, M. H.; Kaur, N.; Comini, E.; Pinna, N., Toward Optimized Radial Modulation of the Space-Charge Region in One-Dimensional SnO2–NiO Core–Shell Nanowires for Hydrogen Sensing. *ACS Appl. Mater. Interfaces* **2020,** *12* (4), 4594-4606.

9.   Tangirala, V. K. K.; Gómez-Pozos, H.; Rodríguez-Lugo, V.; Olvera, M. D. L. L., A Study of the CO Sensing Responses of Cu-, Pt- and Pd-Activated SnO_2 Sensors: Effect of Precipitation Agents, Dopants and Doping Methods. *Sensors (Basel, Switzerland)* **2017,** *17* (5), 1011.

10.   Kwoka, M.; Lyson-Sypien, B.; Kulis, A.; Zappa, D.; Comini, E., Surface Properties of SnO_2 Nanowires Deposited on Si Substrate Covered by Au Catalyst Studies by XPS, TDS and SEM. *Nanomaterials (Basel, Switzerland)* **2018,** *8* (9), 738.

11.   Trung, D. D.; Hoa, N. D.; Tong, P. V.; Duy, N. V.; Dao, T. D.; Chung, H. V.; Nagao, T.; Hieu, N. V., Effective decoration of Pd nanoparticles on the surface of SnO2 nanowires for enhancement of CO gas-sensing performance. *J. Hazard. Mater.* **2014,** *265*, 124-132.

12.   Zhuo, M.; Chen, Y.; Sun, J.; Zhang, H.; Guo, D.; Zhang, H.; Li, Q.; Wang, T.; Wan, Q., Humidity sensing properties of a single Sb doped SnO2 nanowire field effect transistor. *Sens. Actuators, B* **2013,** *186*, 78-83.

13.   Vomiero, A.; Ferroni, M.; Comini, E.; Faglia, G.; Sberveglieri, G., Preparation of Radial and Longitudinal Nanosized Heterostructures of In2O3 and SnO2. *Nano Lett.* **2007,** *7* (12), 3553-3558.

14.   Lettieri, S.; Bismuto, A.; Maddalena, P.; Baratto, C.; Comini, E.; Faglia, G.; Sberveglieri, G.; Zanotti, L., Gas sensitive light emission properties of tin oxide and zinc oxide nanobelts. *J. Non-Cryst. Solids* **2006,** *352* (9), 1457-1460.

15.   Park, S.; Ko, H.; Kim, S.; Lee, C., Role of the Interfaces in Multiple Networked One-Dimensional Core–Shell Nanostructured Gas Sensors. *ACS Appl. Mater. Interfaces* **2014,** *6* (12), 9595-9600.

16.   Degler, D.; Weimar, U.; Barsan, N., Current Understanding of the Fundamental Mechanisms of Doped and Loaded Semiconducting Metal-Oxide-Based Gas Sensing Materials. *ACS Sens.* **2019,** *4* (9), 2228-2249.

17.   Raza, M. H.; Movlaee, K.; Leonardi, S. G.; Barsan, N.; Neri, G.; Pinna, N., Gas Sensing of NiO-SCCNT Core–Shell Heterostructures: Optimization by Radial Modulation of the Hole-Accumulation Layer. *Adv. Funct. Mater.* **2020,** *30* (6), 1906874.

18.   Cheng, C.; Wang, T.-L.; Feng, L.; Li, W.; Ho, K. M.; Loy, M. M. T.; Fung, K. K.; Wang, N., Vertically aligned ZnO/amorphous-Si core–shell heterostructured nanowire arrays. *Nanotechnology* **2010,** *21* (47), 475703.

19.   Tournier, G.; Pijolat, C., Selective filter for SnO2-based gas sensor: application to hydrogen trace detection. *Sens. Actuators, B* **2005,** *106* (2), 553-562.

20.   Ryzhikov, A.; Labeau, M.; Gaskov, A., Al2O3(M=Pt, Ru) catalytic membranes for selective semiconductor gas sensors. *Sens. Actuators, B* **2005,** *109* (1), 91-96.

21.   Weber, M.; Kim, J.-Y.; Lee, J.-H.; Kim, J.-H.; Iatsunskyi, I.; Coy, E.; Miele, P.; Bechelany, M.; Kim, S. S., Highly efficient hydrogen sensors based on Pd nanoparticles supported on boron nitride coated ZnO nanowires. *Journal of Materials Chemistry A* **2019,** *7* (14), 8107-8116.

22.   Weber, M.; Kim, J.-H.; Lee, J.-H.; Kim, J.-Y.; Iatsunskyi, I.; Coy, E.; Drobek, M.; Julbe, A.; Bechelany, M.; Kim, S. S., High-Performance Nanowire Hydrogen Sensors by Exploiting the Synergistic Effect of Pd Nanoparticles and Metal–Organic Framework Membranes. *ACS Appl. Mater. Interfaces* **2018,** *10* (40), 34765-34773.

23.   Nandasiri, M. I.; Jambovane, S. R.; McGrail, B. P.; Schaef, H. T.; Nune, S. K., Adsorption, separation, and catalytic properties of densified metal-organic frameworks. *Coord. Chem. Rev.* **2016,** *311*, 38-52.

24.   Koo, W.-T.; Qiao, S.; Ogata, A. F.; Jha, G.; Jang, J.-S.; Chen, V. T.; Kim, I.-D.; Penner, R. M., Accelerating Palladium Nanowire H2 Sensors Using Engineered Nanofiltration. *ACS Nano* **2017,** *11* (9), 9276-9285.

25.   van den Broek, J.; Weber, I. C.; Güntner, A. T.; Pratsinis, S. E., Highly selective gas sensing enabled by filters. *Materials Horizons* **2021**.

26.   Meng, X.; Zhang, Q.; Zhang, S.; He, Z., The Enhanced H2 Selectivity of SnO2 Gas Sensors with the Deposited SiO2 Filters on Surface of the Sensors. *Sensors* **2019,** *19* (11).

27.   Katsuki, A.; Fukui, K., H2 selective gas sensor based on SnO2. *Sens. Actuators, B* **1998,** *52* (1), 30-37.

28.   Wada, K.; Egashira, M., Hydrogen sensing properties of SnO2 subjected to surface chemical modification with ethoxysilanes. *Sens. Actuators, B* **2000,** *62* (3), 211-219.

29.   Wada, K.; Egashira, M., Improvement of gas-sensing properties of SnO2 by surface chemical modification with diethoxydimethylsilane. *Sens. Actuators, B* **1998,** *53* (3), 147-154.

30.   Gunji, S.; Jukei, M.; Shimotsuma, Y.; Miura, K.; Suematsu, K.; Watanabe, K.; Shimanoe, K., Unexpected gas sensing properties of SiO2/SnO2 core–shell nanofibers under dry and humid conditions. *Journal of Materials Chemistry C* **2017,** *5* (25), 6369-6376.

31.   Miller, D. R.; Akbar, S. A.; Morris, P. A., Nanoscale metal oxide-based heterojunctions for gas sensing: A review. *Sens. Actuators, B* **2014,** *204*, 250-272.

32.   Comini, E.; Baratto, C.; Faglia, G.; Ferroni, M.; Vomiero, A.; Sberveglieri, G., Quasi-one dimensional metal oxide semiconductors: Preparation, characterization and application as chemical sensors. *Prog. Mater Sci.* **2009,** *54* (1), 1-67.

33.   Kaur, N.; Comini, E.; Zappa, D.; Poli, N.; Sberveglieri, G., Nickel oxide nanowires: vapor liquid solid synthesis and integration into a gas sensing device. *Nanotechnology* **2016,** *27* (20), 205701.

34.   Penner, R. M., Chemical Sensing with Nanowires. *Annual Review of Analytical Chemistry* **2012,** *5* (1), 461-485.

35.   Favier, F.; Walter, E. C.; Zach, M. P.; Benter, T.; Penner, R. M., Hydrogen Sensors and Switches from Electrodeposited Palladium Mesowire Arrays. *Science* **2001,** *293* (5538), 2227.

36.   Kaur, N.; Singh, M.; Comini, E., One-Dimensional Nanostructured Oxide Chemoresistive Sensors. *Langmuir* **2020,** *36* (23), 6326-6344.

37.   Singh, M.; Kaur, N.; Drera, G.; Casotto, A.; Sangaletti, L.; Comini, E., SAM Functionalized ZnO Nanowires for Selective Acetone Detection: Optimized Surface Specific Interaction Using APTMS and GLYMO Monolayers. *Adv. Funct. Mater.* **2020,** *30* (38), 2003217.

38.   Comini, E.; Faglia, G.; Ferroni, M.; Ponzoni, A.; Vomiero, A.; Sberveglieri, G., Metal oxide nanowires: Preparation and application in gas sensing. *J. Mol. Catal. A: Chem.* **2009,** *305* (1), 170-177.

39.   Marichy, C.; Russo, P. A.; Latino, M.; Tessonnier, J.-P.; Willinger, M.-G.; Donato, N.; Neri, G.; Pinna, N., Tin Dioxide–Carbon Heterostructures Applied to Gas Sensing: Structure-Dependent Properties and General Sensing Mechanism. *J. Phys. Chem. C* **2013,** *117* (38), 19729-19739.

40.   Ziegler, J. M.; Andoni, I.; Choi, E. J.; Fang, L.; Flores-Zuleta, H.; Humphrey, N. J.; Kim, D.-H.; Shin, J.; Youn, H.; Penner, R. M., Sensors Based Upon Nanowires, Nanotubes, and Nanoribbons: 2016–2020. *Anal. Chem.* **2021,** *93* (1), 124-166.

41.   Marichy, C., Pucci, A., Willinger, M.-G. and Pinna, N, Coating of Carbon Nanotubes. In *In Atomic Layer Deposition of Nanostructured Materials*, Knez, N. P. a. M., Ed. Wiley-VCH: 2012; pp 327-343.

42.   Marichy, C.; Bechelany, M.; Pinna, N., Atomic Layer Deposition of Nanostructured Materials for Energy and Environmental Applications. *Adv. Mater.* **2012,** *24* (8), 1017-1032.

43.   Marichy, C.; Pinna, N., Atomic Layer Deposition to Materials for Gas Sensing Applications. *Adv. Mater. Interfaces* **2016**, *3* (21), 1600335.

44.   Ponti, A.; Raza, M. H.; Pantò, F.; Ferretti, A. M.; Triolo, C.; Patanè, S.; Pinna, N.; Santangelo, S., Structure, Defects, and Magnetism of Electrospun Hematite Nanofibers Silica-Coated by Atomic Layer Deposition. *Langmuir* **2020**, *36* (5), 1305-1319.

45.   Raza, M. H.; Movlaee, K.; Wu, Y.; El-Refaei, S. M.; Karg, M.; Leonardi, S. G.; Neri, G.; Pinna, N., Tuning the NiO Thin Film Morphology on Carbon Nanotubes by Atomic Layer Deposition for Enzyme-Free Glucose Sensing. *ChemElectroChem* **2019,** *6* (2), 383-392.

46.   Wu, Y.; Raza, M. H.; Chen, Y.-C.; Amsalem, P.; Wahl, S.; Skrodczky, K.; Xu, X.; Lokare, K. S.; Zhukush, M.; Gaval, P.; Koch, N.; Quadrelli, E. A.; Pinna, N., A self-limited atomic layer deposition of WS2 based on the chemisorption and reduction of bis(t-butylimido)bis(dimethylamino) complexes. *Chem. Mater.* **2019**.

47.   Kaur, N.; Zappa, D.; Ferroni, M.; Poli, N.; Campanini, M.; Negrea, R.; Comini, E., Branch-like NiO/ZnO heterostructures for VOC sensing. *Sens. Actuators, B* **2018,** *262*, 477-485.

48.   Bachmann, J.; Zierold, R.; Chong, Y. T.; Hauert, R.; Sturm, C.; Schmidt-Grund, R.; Rheinländer, B.; Grundmann, M.; Gösele, U.; Nielsch, K., A Practical, Self-Catalytic, Atomic Layer Deposition of Silicon Dioxide. *Angew. Chem. Int. Ed.* **2008,** *47* (33), 6177-6179.

49.   Staerz, A.; Liu, Y.; Geyik, U.; Brinkmann, H.; Weimar, U.; Zhang, T.; Barsan, N., The effect of platinum loading on WO3 based sensors. *Sens. Actuators, B* **2019,** *291*, 378-384.

50.   Staerz, A.; Kim, T.-H.; Lee, J.-H.; Weimar, U.; Barsan, N., Nanolevel Control of Gas Sensing Characteristics via p–n Heterojunction between Rh2O3 Clusters and WO3 Crystallites. *J. Phys. Chem. C* **2017,** *121* (44), 24701-24706.

51.   Liu, W.; Xu, L.; Sheng, K.; Chen, C.; Zhou, X.; Dong, B.; Bai, X.; Zhang, S.; Lu, G.; Song, H., APTES-functionalized thin-walled porous WO3 nanotubes for highly selective sensing of NO2 in a polluted environment. *Journal of Materials Chemistry A* **2018,** *6* (23), 10976-10989.

52.   Liang, Y.; Tracy, C.; Weisbrod, E.; Fejes, P.; Theodore, N. D., Effect of SiO2 incorporation on stability and work function of conducting MoO2. *Appl. Phys. Lett.* **2006,** *88* (8), 081901.

53.   Afanas'ev, V. V., Electron Band Alignment at Interfaces of Semiconductors with Insulating Oxides: An Internal Photoemission Study. *Advances in Condensed Matter Physics* **2014,** *2014*, 301302.

54.   Choi, M. S.; Na, H. G.; Bang, J. H.; Mirzaei, A.; Han, S.; Lee, H. Y.; Kim, S. S.; Kim, H. W.; Jin, C., SnO2 nanowires decorated by insulating amorphous carbon layers for improved room-temperature NO2 sensing. *Sens. Actuators, B* **2021,** *326*, 128801.

55.   Hu, J.; Yang, J.; Wang, W.; Xue, Y.; Sun, Y.; Li, P.; Lian, K.; Zhang, W.; Chen, L.; Shi, J.; Chen, Y., Synthesis and gas sensing properties of NiO/SnO2 hierarchical structures toward ppb-level acetone detection. *Mater. Res. Bull.* **2018,** *102*, 294-303.

56.   Comini, E., Metal oxide nano-crystals for gas sensing. *Anal. Chim. Acta* **2006,** *568* (1), 28-40.

57.   Barsan, N.; Weimar, U., Conduction Model of Metal Oxide Gas Sensors. *J. Electroceram.* **2001,** *7* (3), 143-167.

58.   Comini, E., Metal oxides nanowires chemical/gas sensors: recent advances. *Materials Today Advances* **2020,** *7*, 100099.

59.   Feng, C. D.; Shimizu, Y.; Egashira, M., Effect of Gas Diffusion Process on Sensing Properties of SnO2 Thin Film Sensors in a SiO2 / SnO2 Layer-Built Structure Fabricated by Sol-Gel Process. *J. Electrochem. Soc.* **1994,** *141* (1), 220-225.